of the manuscript. M.K. and H.M. thank the Fonds der Chemischen Industrie for a fellowship.

Supplementary Material Available: Tables S1-S5 containing positional and anisotropic thermal parameters, bond distances and angles, and torsion angles from the X-ray structure of II, Tables S7-S10 containing atomic coordinates of averaged MD structures of I from water simulations and II from in vacuo calculations, Tables S11-S13 containing calculated distances, dihedral angles, and hydrogen bonds from MD simulations of I in DMSO, and Tables S14 and S15 containing hydrogen bonds from different MD simulations of I (in water) and II (in vacuo) (20 pages); Table S6 containing observed and calculated structure factors (28 pages). Ordering information is given on any current masthead page.

Conformation of Cyclic Analogues of Substance P: NMR and Molecular Dynamics in Dimethyl Sulfoxide

Juris Saulitis,[‡] Dale F. Mierke, Gerardo Byk,[†] Chaim Gilon,[†] and Horst Kessler*

Contribution from the Organisch Chemisches Institut, Technische Universität München, Lichtenbergstrasse 4, 8046 Garching, Germany, and Department of Organic Chemistry, Hebrew University of Jerusalem, Jerusalem 91904, Israel. *Received May 20, 1991*

Abstract: The conformational analysis of two cyclic analogues of substance P has been carried out using NMR spectroscopy and restrained molecular dynamics calculations. The cyclic analogues, cyclo[-$(CH_2)_m$-NH-CO-$(CH_2)_n$-CO-Arg-Phe-Phe-N-]-CH_2-CO-Leu-Met-NH_2 (with m, n = 3, 2 and 3, 3), show a large percentage of cis configurational isomers (18 and 22%) about the substituted amide. The additional isomers lead to severe spectral overlap of the proton resonances. Using the carbon resonances and the associated large chemical shift dispersion allows for the unambiguous assignment of all proton resonances. From the NOEs, temperature gradients, and coupling constants the conformation of the cyclic portion of the molecule is well-determined. The structures obtained from the experimental study were refined with NOE-restrained molecular dynamics. The computer simulations were carried out in dimethyl sulfoxide, the same solvent used in the experimental study. The dynamic stability of the refined conformations was evaluated by performing an extended, free MD simulation (400 ps) in dimethyl sulfoxide. The comparison of the interproton distances from the NOEs (two-spin approximation) with the effective distances from the free MD simulation is introduced as a possible tool to test the quality of obtained structures.

Introduction

Substance P (SP) is an undecapeptide, Arg-Pro-Lys-Pro-Gln-Gln-Phe-Phe-Gly-Leu-Met-NH_2, belonging to the tachykinins, a family of peptides sharing the common C-terminal amino acid sequence Phe-Xaa-Gly-Leu-Met-NH_2 and a broad range of biological activities.[1] In fact, the C-terminal hexapeptide of SP, Gln-Phe-Phe-Gly-Leu-Met-NH_2, retains much of the biological activity of the native molecule. The role of SP in the transmission or modulation of pain stimuli is of particular interest.[2] Three different classes of receptors for SP have been identified and cloned (neurokinin receptors NK-1, NK-2, and NK-3).[3] The wide range of physiological activity of SP has been attributed to the lack of selectivity of SP for a particular receptor type. The conformational flexibility of the linear peptide can account for the lack of selectivity.

One method to reduce the conformational freedom of a peptide and greatly increase the selectivity for receptors is cyclization. This method has been applied successfully to many different peptide systems.[4] Therefore, the goals in the cyclization of the neuropeptide substance P were 2-fold. The first goal was to develop a highly selective, metabolically stable analogue. The second goal was to impose conformational constraint in order to lock the peptide in a bioactive conformation that fits each tachykinin receptor.

However, the C-terminal hexapeptide of SP is resistant to cyclization. The common methods for cyclization including end-to-end, end-to-side chain, and side chain-to-side chain lead to analogues with little or no activity.[5] The side chains commonly used for cyclization cannot be modified and, in addition, the C-terminal portion must be free as an amide.

To overcome the limitations of the conventional modes of cyclization, we have recently[6] introduced a new general concept for

* To whom correspondence should be addressed at the Technische Universität München.
‡ Deceased September 9, 1991.
† Hebrew University of Jerusalem.

(1) Pernow, B. *Pharmacol. Rev.* **1983**, *35*, 85-141.
(2) Nicoll, R. A.; Schenker, C.; Leeman, S. E. *Annu. Rev. Neurosci.* **1980**, *3*, 227-268.
(3) (a) *Trends Pharm. Sci. Receptor Nomenclature, Supplement* **1990**, 25. (b) Lee, C. M.; Iverson, L. L.; Hanley, M. R.; Sandberg, B. E. B. *N. S. Arch. Pharmacol.* **1982**, *318*, 281-287. (c) Laufer, R.; Wormser, U.; Friedman, Z. Y.; Gilon, C.; Chorev, M.; Selinger, Z. *Proc. Natl. Acad. Sci. U.S.A.* **1985**, *82*, 7444-7448. (d) Quirion, R.; Dam, T. V. *Neuropeptides* **1985**, *6*, 191-204. (e) Buck, S. K.; Shatzer, S. A. *Life Sci.* **1988**, *44*, 2701-2705. (f) Regoli, D.; Nantel, F. *Biopolymers* **1991**, *31*, 777-783. (g) Masu, Y.; Nakayama, K.; Takami, H.; Harada, Y.; Kuno, M.; Nakanishi, S. *Nature* **1987**, *329*, 836-838. (h) Yokota, Y.; Yoshiki, S.; Kohichi, T.; Fujiwara, T.; Tsuchida, K.; Shigemoto, R.; Kakizuka, A.; Ohkubo, H.; Nakanishi, S. *J. Biol. Chem.* **1989**, *264*, 17649-17653. (i) Shigemoto, R.; Yokota, Y.; Tsuchida, K.; Nakanishi, S. *J. Biol. Chem.* **1990**, *265*, 623-628.
(4) There are many examples within the peptide field: enkephalins (Schiller, P. W. In *The Peptides*; Udenfriend, S., Meienhofer, J., Eds.; Academic Press: Orlando, FL, 1984; Vol. 6, pp 219-298. Hruby, V. J.; Al-Obeidi, F.; Kazmierski, W. *Biochem. J.* **1990**, *268*, 249-262), somatostatins (Veber, D. H.; Holly, F. W.; Paleveda, W. J.; Nutt, R. F.; Bergstrand, S. J.; Torchiana, M.; Glitzer, M. S.; Saperstein, R.; Hirschmann, R. *Proc. Natl. Acad. Sci. U.S.A.* **1978**, *75*, 2636-2640), thymopoietin (Lautz, J.; Kessler, H.; Boelens, R.; Kaptein, R.; van Gunsteren, W. F. *Int. J. Peptide Protein Res.* **1987**, *30*, 404-414. Kessler, H.; Kutcher, B. *Tetrahedron Lett.* **1985**, *26*, 177-180), and RGD peptides (Aumailley, M.; Gurrath, M.; Müller, G.; Calvete, J.; Timpl, R.; Kessler, H. *FEBS Lett.* **1991**, *291*, 50-54).
(5) (a) Neubert, K.; Hartrodt, B.; Mehlis, B.; Ruger, M.; Bergman, J.; Lindau, J.; Jakubke, H. D.; Barth, A. *Pharmazie* **1985**, *40*, 617. (b) Chassaing, G.; Lavielle, S.; Ploux, O.; Julien, C.; Convert, O.; Marquet, A.; Beaujouan, J. C.; Torrens, Y.; Glowinsky, J. In *Peptides 1984*; Ragnarsson, U., Ed.; Almquist & Wiksell: Stockholm, 1985; p 345. (c) Sandberg, B. E. B.; Bishai, W. R.; Hauna, P. In *Peptides 1984*; Ragnarsson, U., Ed.; Almquist & Wiksell: Stockholm, 1985; p 369. (d) Theodoropoulus, D.; Poulus, C.; Calos, D.; Cordopatis, P.; Escher, E.; Mizrahi, J.; Regoli, D.; Dalietos, D.; Furst, A.; Lee, T. *J. Med. Chem.* **1985**, *28*, 1536. (e) Darman, P.; Landis, G.; Smits, J.; Hirning, L.; Gulya, K.; Yamamura, I.; Burks, T.; Hruby, V. J. *Biochem. Biophys. Res. Commun.* **1985**, *127*(2), 656. (f) Mutulis, F.; Mutulc, I.; Maurops, G.; Seckacis, I.; Grigor'eve, V. D.; Kakaine, E.; Golubeva, V. V.; Myshlyakova, N. V.; Cipens, G. *Bioorg. Khim.* **1985**, *11*, 1276.

0002-7863/92/1514-4818$03.00/0

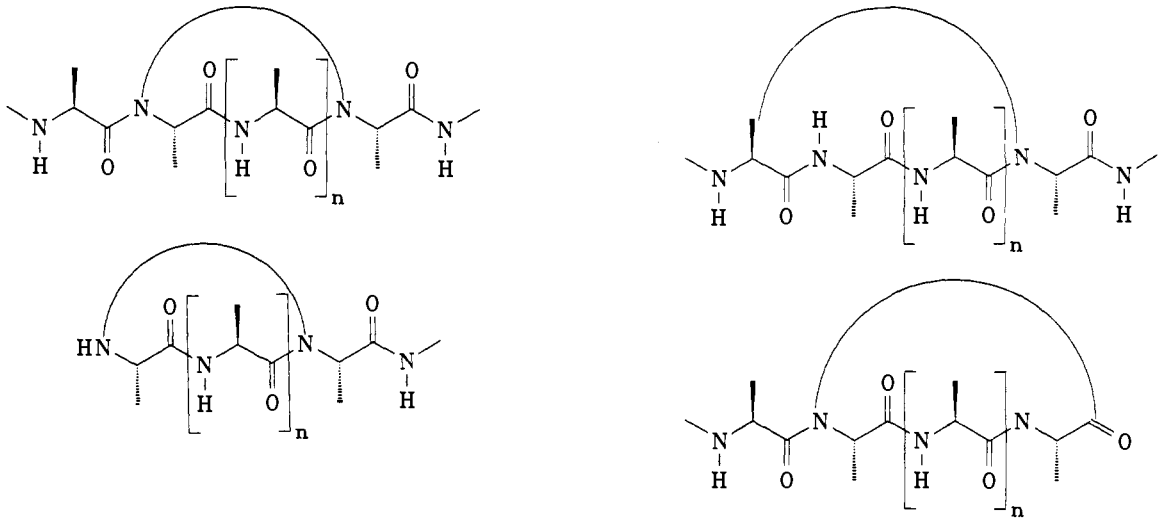

Figure 1. Illustration of the concept of N-backbone cyclization: (upper left) N to N-backbone, (upper right) N-backbone to side chain and (lower) N-backbone to the end groups. A number of linkers have been utilized (e.g. disulfide [-R-S-S-R-], amide [-R-CO-NH-R-]).

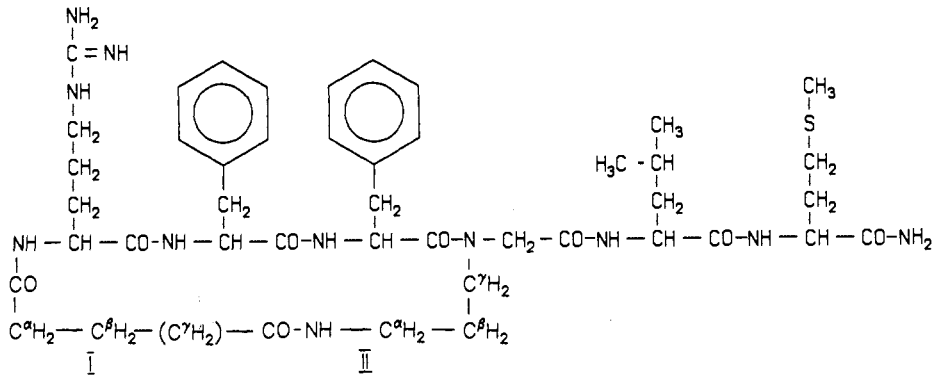

Figure 2. The structure and nomenclature of the SP **1** and **2** analogues. SP **2** has one additional methylene group within the bridging region, $C^{\gamma}H_2$, which is shown in parentheses. The bridging region connecting Arg and NGly consists of two fragments I and II, separated by the amide bond.

long-range cyclization of peptides called "backbone cyclization". According to this concept, cyclization is achieved by joining the N^{α} atoms of a peptide backbone to each other, or to side chains, or to the amino or carboxy ends through an appropriate linker. The concept of backbone cyclization is shown in Figure 1.

This new method of cyclization was applied to the hexapeptide WS Septide (Ac[Arg^6,Pro^9]SP_{6-11}) which is a selective NK-1 SP analogue (EC_{50} (nM): NK-1, 3.0; NK-2, >200 000; NK-3, >200 000). The design of the N-backbone cyclization of WS Septide was based on a model derived from an NMR study[7] carried out in dimethyl sulfoxide (DMSO) and structure activity relationship studies. A series of N-backbone cyclic analogues of WS Septide with different ring sizes were synthesized. It was found that the activity and selectivity of these cyclic analogues at the NK-1 receptor depends on the ring size, with optimal activity and selectivity with 19- and 20-membered rings (corresponding to SP **1** and **2**, respectively, Figure 2). The analogues have biological profiles similar to that of the WS Septide (EC_{50} (nM): SP **1**—NK-1, 180; NK-2, >50000; NK-3, >10000; SP **2**—NK-1, 11; NK-2, >50 000; NK-3, >10 000). The cyclic analogues also showed protracted activity in various tissues as compared to the very fast degradation rate of the WS Septide.[6]

Here we report the ^1H and ^{13}C NMR investigation of SP **1** and **2** in DMSO. The biological relevance of the examination of peptides in DMSO is currently in dispute. However, the receptors for these molecules are thought to be composed of both lipophilic and polar portions, properties that DMSO can certainly mimic better than aqueous solutions. The structures derived from the NMR study were then refined using distance-restrained molecular dynamics (MD). The MD simulations were carried out using DMSO as the solvent and incorporating potential parameters recently developed.[8] Further, free MD simulations in solvent were carried out to examine the energetic stability and quality of the resulting conformations. These steps are shown in Figure 3 in order to illustrate the sequence of procedures. The right side of the diagram is traditional, frequently used to obtain structures from a set of NOE-derived interproton distances. In the present paper the extended free MD simulation, left side of the diagram,

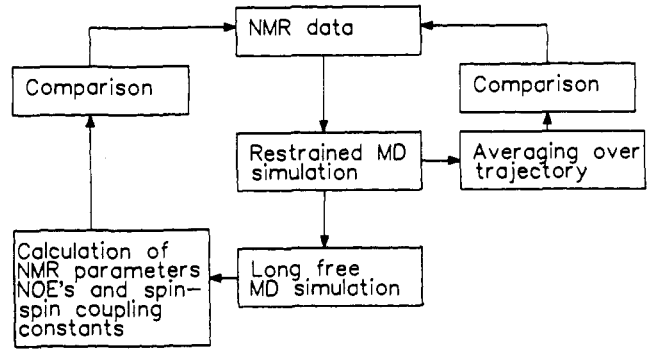

Figure 3. A diagram illustrating the procedure used to obtain conformations of SP **1** and **2** and to test the quality of the structures. The left side of the scheme points out the reproduction of the averaged NMR data from the trajectory of the free MD simulation.

(6) (a) Gilon, C.; Halle, D.; Chorev, M.; Selinger, Z.; Byk, G. *Biopolymers* **1991**, *31*, 745–750. (b) Halle, D.; Goldschmidt, R.; Byk, G.; Chorev, M.; Selinger, Z.; Gilon, C. In preparation.

(7) (a) Wormser, U.; Laufer, R.; Hart, Y.; Chorev, M.; Gilon, C.; Selinger, Z. *EMBO J.* **1986**, *5*, 2805–2809. (b) Livian-Teitelbaum, D.; Kolodny, N.; Chorev, M.; Selinger, Z.; Gilon, C. *Biopolymers* **1989**, *28*, 51–64.

(8) Mierke, D. F.; Kessler, H. *J. Am. Chem. Soc.* **1991**, *113*, 9466–9470.

is introduced to imitate the dynamics of the peptide in solution. The rather good reproducibility of the distances calculated from the NOEs during the free simulation indicates that the derived conformational model is an acceptable solution of the experimental data.

Experimental Methods

Proton and carbon spectra were recorded on Bruker AMX-500 and 600 spectrometers, operating at 500 and 600 MHz proton resonance frequencies. Data were processed on Bruker X32 work stations using the UXNMR program. The sample concentrations were 18 and 31 mM for SP **1** and **2**, respectively, in 5-mm NMR tubes using DMSO-d_6 from Aldrich. All spectra were recorded at 303 K except for the temperature coefficients which were measured for the amide proton resonances by variation of the temperature from 303 to 333 K.

The ROESY[9,10] and TOCSY[11,12] spectra were recorded at 500 MHz with 32 scans, a relaxation delay of 2 s, 512 t_1 increments, and 2048 data points in t_2. The spectral width in both dimensions was 5020 Hz, and after zero filling the final size of the data matrix was 1024 × 2048. Apodization with a squared sine bell function shifted by $\pi/3$ was used in both dimensions. An MLEV-17[12] mixing scheme of 32 ms with a 10-kHz spin locking field strength was used for the TOCSY while a continuous wave mixing of 150 ms (6 kHz cw spin locking field strength) was used for the ROESY.

The NOESY[13] spectra were recorded at 600 MHz with 600–700 points in the t_1 dimension, 32–48 scans, a relaxation delay of 2 s, and 2048 data points in t_2. The spectral width in both dimensions was 7020 Hz, and after zero filling the final size of the data matrix was 1024 × 4096. Apodization with a squared sine bell function shifted by $\pi/3$ was used in both dimensions. After Fourier transform a third-order baseplane correction was usually performed. The mixing time was varied randomly by 10%. Spectra with different mixing times were collected: five for SP **1** with mixing times of 100, 120, 150, 180, and 200 ms and three for SP **2** with mixing times of 100, 150, and 180 ms. The different mixing times were used to evaluate the linear buildup of the NOE and the appropriateness of the two-spin approximation. The integral intensities of cross peaks were measured by the integration routine within the UXNMR program.

The complementary E. COSY[14-16] spectra were recorded at 500 MHz with 1024 t_1 increments and 4096 points in the t_2 dimension, a relaxation delay of 2.5 s, and a spectral width of 2500 Hz in both dimensions. The final 1024 × 8192 data matrix, after zero filling, was apodizated before Fourier transformation by a squared sine bell function shifted by $\pi/2$. Proton coupling constants were extracted from 1D sections in E. COSY spectra taken along the f_2 axis. The simulation of E. COSY spectra was carried out on a Bruker X32 computer using the SMART program.[17]

The ^{1}H,^{13}C HMQC[18-21] and DEPT-HMQC[22,23] spectra with the BIRD sequence were recorded at 500 MHz (125.8 MHz for ^{13}C) with a spectral width of 6250 Hz in f_2 (^{1}H) and 4166 Hz in f_1 (^{13}C), a relaxation delay of 184 ms, 160 scans, and GARP decoupling. The signal from the BIRD sequence was minimized with a delay of 198 ms. The DEPT proton pulse was $\pi/2$ or $\pi/3$ to select CH, CH_2, and CH_3 or CH_2 carbon resonances. The experimental data matrix was zero filled to 1024 × 4096 complex points. The ^{1}H,^{13}C DEPT-HMQC-TOCSY[22,23] spectra were collected in a similar manner only with the addition of an MLEV-17 isotropic mixing period of 32 ms with a spin locking field of 10 kHz. A $\pi/2$ shifted sine bell apodization in f_2 and exponential 5 Hz line broadening in f_1 were applied before the phase-sensitive Fourier transformation.

The energy minimizations and MD simulations were carried out using the GROMOS program.[24] The initial coordinates for SP **1** and **2** were built using the MOLEDT program from BIOSYM. The corresponding cis (minor) analogues were created by addition of a forcing potential to the Phe^3-NGly amide bond (force constant 1 kJ mol^{-1} Å^{-2}) and energy minimization. The forcing potential placed on the amide was then removed and the peptides energy minimized. The peptides were placed in a periodic truncated octahedron of 10 200 Å^3 containing 68–71 DMSO solvent molecules.[8,25] The system was then energy minimized for 200 steps of steepest descents to remove any high-energy contacts.

The MD simulations were carried out using a step size of 1 fs employing the SHAKE method.[26] The nonbond interactions were updated every 20 steps with a cutoff distance of 10 Å. For the first 5 ps the temperature was maintained at 1000 K by strong coupling to a temperature bath (coupling relaxation time of 10 fs).[27] The NOE and dihedral restraining functions were applied with force constants of 20 and 0.25 kJ mol^{-1} Å^{-2}, respectively. The upper and lower NOE bound restraints were set to plus and minus 5% of the experimentally determined values, respectively. A weak constraining function taking into account the NH–C$^\alpha$H coupling constant (see below) was placed on the ϕ of Phe^2 of all of the structures to −120°, Arg of the major isomer of SP **1** to −60°, and Phe^3 of the minor isomer of SP **2** to −60°. After these 5 ps, the temperature was reduced to 300 K and the system allowed to equilibrate for 5 ps while maintaining the experimental constraints and strong temperature coupling. The NOE and dihedral force constants were then reduced to 10 and 0.05 kJ mol^{-1} Å^{-2}, respectively, the temperature coupling set to 200 fs, and the dynamics continued for 100 ps. A structure was saved every 0.5 ps during the simulation for analysis.

For the major isomers of SP **1** and **2**, the experimental restraints were removed and the simulations continued for an additional 400 ps. The effective distance between atoms involved in NOEs was determined by calculating the inverse cube of the distance, r^{-3}, for each configuration and then averaging this value over the trajectory. The expected coupling constants from torsion angles were calculated in a similar manner using coefficients of 8.6, −1.0, and 0.4 in a modified Karplus equation relating proton vicinal coupling constants and interproton dihedral angles.[28-30] All computer simulations were carried out on Silicon Graphics 4D/240SX and 4D/70GTB computers.

Results

The one-dimensional proton spectrum of SP **1** displayed two distinct sets of resonances in the amide proton region with integrated populations of 78 and 22%. In NOESY and ROESY spectra, cross peaks between the resonances of the major and minor isomers were observed. The peaks in the ROESY spectrum were of the same sign as the diagonal, clearly indicating the exchange between the two isomers. The cross peaks from the chemical exchange are illustrated in the NOESY spectrum (Figure S1, supplementary material). Two isomers exchanging on the NMR time scale were also identified in the proton spectra of SP **2** with relative populations of 82 and 18%.

The NOEs measured for SP **2** allowed for the identification of the minor isomer: an NOE between the α protons of Phe^3 and NGly shows that the peptide bond between these residues is in a cis orientation. Such NOEs are commonly used to indicate a cis configuration of amide bonds.[31,32] The peptide bond between

(9) (a) Bothner-By, A. A.; Stephens, K. L.; Lee, J.; Warren, C. D.; Jeanloz, R. W. *J. Am. Chem. Soc.* **1984**, *106*, 811–813. (b) Bax, A.; Davis, D. G. *J. Magn. Reson.* **1985**, *63*, 207–213.
(10) Kessler, H.; Griesinger, G.; Kerssebaum, R.; Wagner, K.; Ernst, R. R. *J. Am. Chem. Soc.* **1987**, *109*, 607–609.
(11) (a) Braunschweiler, L.; Ernst, R. R. *J. Magn. Reson.* **1983**, *53*, 521–528. (b) Bax, A.; Davis, D. G. *J. Am. Chem. Soc.* **1985**, *107*, 2820–2821.
(12) Bax, A.; Davis, D. G. *J. Magn. Reson.* **1985**, *65*, 355–360.
(13) Jeener, J.; Meier, B. H.; Bachmann, P.; Ernst, R. R. *J. Chem. Phys.* **1979**, *71*, 4546–4553.
(14) Griesinger, C.; Sørensen, O. W.; Ernst, R. R. *J. Am. Chem. Soc.* **1985**, *107*, 6394–6396.
(15) Griesinger, C.; Sørensen, O. W.; Ernst, R. R. *J. Chem. Phys.* **1986**, *85*, 6837–6852.
(16) Griesinger, C.; Sørensen, O. W.; Ernst, R. R. *J. Magn. Reson.* **1987**, *75*, 474–492.
(17) Studer, W. *J. Magn. Reson.* **1988**, *77*, 424–438.
(18) Müller, L. *J. Am. Chem. Soc.* **1979**, *101*, 4481–4484.
(19) Bax, A.; Griffey, R. H.; Hawkins, L. B. *J. Magn. Reson.* **1983**, *55*, 301–315.
(20) (a) Lerner, A.; Bax, A. *J. Magn. Reson.* **1986**, *69*, 375–380. (b) Bax, A.; Summers, M. F. *J. Am. Chem. Soc.* **1986**, *108*, 2093–2094.
(21) Bax, A.; Subramaniam, S. *J. Magn. Reson.* **1986**, *67*, 565–568.
(22) Kessler, H.; Schmieder, P. *Biopolymers* **1991**, *31*, 621–629.
(23) Kessler, H.; Schmieder, P.; Kurz, M. *J. Magn. Reson.* **1989**, *85*, 400–405.
(24) van Gunsteren, W. F.; Berendsen, H. J. C. *Groningen Molecular Simulation (GROMOS) Library Manual*; Biomos, B. V., Nijenborgh 16, NL 9747 AG Groningen; pp 1–229.
(25) Rao, B. G.; Singh, U. C. *J. Am. Chem. Soc.* **1990**, *112*, 3802–3811.
(26) van Gunsteren, W. F.; Berendsen, H. J. C. *Mol. Phys.* **1977**, *34*, 1311–1321.
(27) Berendsen, H. J. C.; Postma, J. P. M.; van Gunsteren, W. F.; DiNola, A.; Haak, J. R. *J. Chem. Phys.* **1984**, *81*, 3684–3690.
(28) Haasnoot, C. A. G.; de Leeuw, F. A. A. M.; de Leeuw, H. P. M.; Altona, C. *Org. Magn. Reson.* **1981**, *15*, 43–51.
(29) Haasnoot, C. A. G.; de Leeuw, F. A. A. M.; de Leeuw, H. P. M.; Altona, C. *Tetrahedron* **1980**, *36*, 2783–2791.
(30) Karplus, M.; Petsko, G. A. *Nature* **1990**, *347*, 631–639.
(31) Arsenjev, A. S.; Kondakov, V. I.; Maiorov, V. N.; Volkova, T. M.; Grishin, E. V.; Bystrov, V. F.; Ovchinnikov, Yu. A. *Bioorg. Khim.* **1983**, *9*, 768–793.

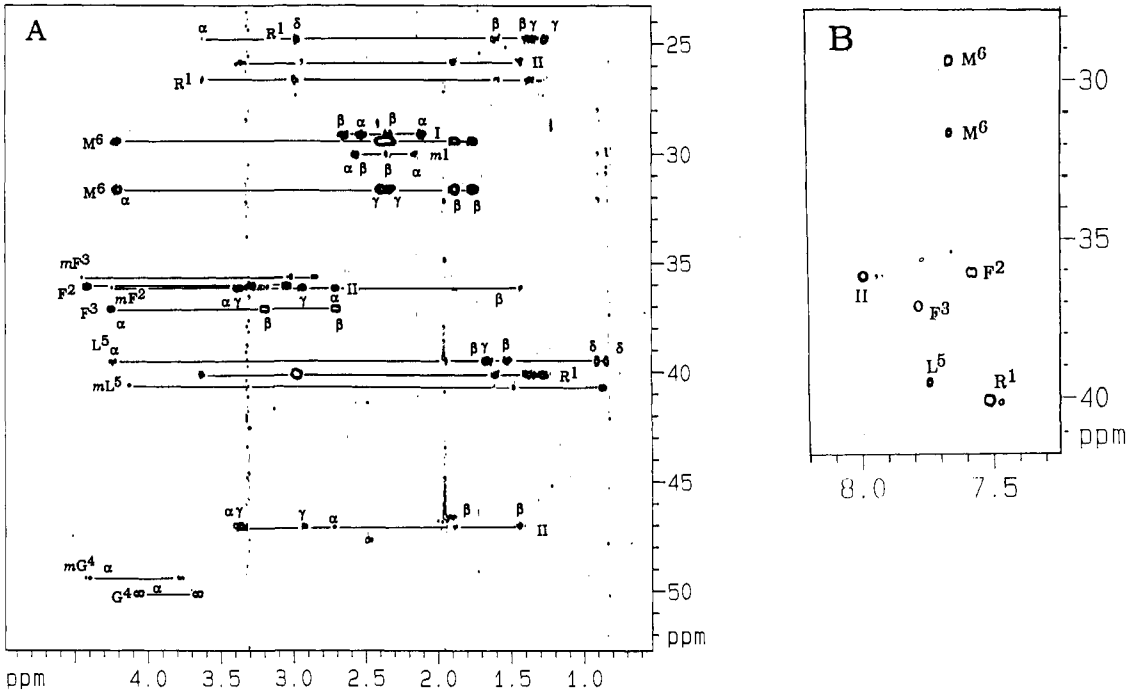

Figure 4. Expanded portions of an inverse DEPT edited ^1H–^{13}C HMQC-TOCSY spectrum of SP **1** recorded at 303 K at 500 MHz: (A) aliphatic proton region and (B) amide proton region.

Phe^3 and NGly in the major isomer is in a trans orientation illustrated by an NOE between the α proton of Phe^3 and $C^\gamma H_2$ of fragment II of the bridging region. The same NOE was observed for the major isomer of SP **1**. The α–α NOE of the minor isomer of SP **1** was not observed because of overlap of the Phe^3 and NGly resonances.

The assignment of the proton resonances was carried out following standard procedures[32] using the homonuclear NOESY, ROESY, TOCSY, and E. COSY techniques. Even with these small peptides, the proton assignments were not complete because of severe spectral overlap and the presence of the two isomers. The relatively small populations of the minor isomer of SP **1** and **2** resulted in a lack of some cross peaks in the homonuclear J correlated and NOESY spectra introducing uncertainties in the assignment of the minor isomer resonances. To overcome these problems a ^{13}C NMR spectrum and the large chemical shift dispersion of the carbon resonances were utilized. The inverse correlation methods DEPT-HMQC and DEPT-HMQC-TOCSY were used to obtain assignment of the aliphatic carbon resonances and then the unambiguous proton assignments.

The use of the inverse ^1H,^{13}C DEPT HMQC in the assignment is illustrated in Figure 4. The HMQC spectrum (Figure S2, supplementary material) although greatly improved over the proton spectra still contains many overlapping resonances. The multiquantum-DEPT editing of the carbon dimension results in a simplified spectrum (Figure 4, A and B). The considerably smaller intensities of the cross peaks in the 2D heteronuclear spectra of the minor isomer (and different chemical shifts of the carbon resonances of the major and minor isomers) allowed for easy identification. The inverse ^1H,^{13}C HMQC experiments are extremely useful in the assignment of minor isomer resonances, a problem often encountered when studying proline-containing peptides.[33] Undoubtedly, the proper relaxation delay before and after the BIRD scheme in the pulse sequence of the ^1H,^{13}C HMQC experiment[21] is a critical factor in the effectiveness of these experiments.

After the assignment of the resonances of each residue, the last step is the sequence analysis carried out by the NOESY spectra, using the NOE cross peaks between $C^\alpha_i H$–$N_{i+1}H$, H_iH–$N_{i+1}H$ and $C^\beta_i H$–$N_{i+1}H$ protons. An expanded portion of the NOESY spectrum illustrating the $C^\alpha_i H$–$N_{i+1}H$ NOEs measured for SP **2** is shown in Figure 5. The proton and aliphatic carbon chemical shifts for SP **1** and **2** are given in the supplementary material (Tables S1–S4).

The temperature coefficients of the amide protons were measured at six temperatures from 303 to 333 K. During the change in temperature the α-protons were monitored to ensure that conformational changes did not occur at the elevated temperature. In addition, there was no observable difference in the populations of the major or minor isomer with this change in temperature. The temperature coefficients are listed in Table I. The values

Table I. Temperature Dependence of the Amide Protons of SP **1** and **2** in DMSO[a]

isomer		Arg^1	Phe^2	Phe^3	Leu^5	Met^6	II
SP **1**	major	8.0	3.3	0.1	3.1	8.1	8.8
	minor	9.3	−0.9	2.9	8.9	10.2	8.1
SP **2**	major	4.4	0.8	5.5	5.4	6.2	5.3
	minor	4.6	−1.4	7.2	5.3	7.1	4.2

[a] The temperature coefficients are given in negative parts per billion per K.

Table II. Proton Vicinal Coupling Constants of SP **1** and **2** in DMSO at 303 K[a]

	^3J(NH,C$^\alpha$H)		^3J(C$^\alpha$H,C$^\beta$H)[c]	
residue	**1**	**2**	**1**	**2**
Arg^1	5.4	7.1	9.2, 6.0	9.2, 6.0
	(6.2)	(7.7)	(9.2, 6.0)	(9.2, 6.0)
Phe^2	9.1	8.5	3.1 *S*, 11.8 *R*	4.0 *R*, 8.4 *S*
	(8.9)	(8.9)	(4.4 *R*, 10.8 *S*)	(4.5 *S*, 8.9 *R*)
Phe^3	5.6	7.5	5.9 *R*, 8.4 *S*	6.1 *S*, 8.0 *R*
	(7.4)	(5.1)	(4.0 *R*, 10.1 *S*)	(3.3 *S*, 10.1 *R*)
Leu^5	7.4	7.8	10.1, 5.1	10.1, 5.2
	(7.7)	(8.0)	(9.5, 5.8)	(9.4, 5.8)
Met^6	8.0	8.0	[b]	
	(8.3)	(8.1)	[b]	

[a] Coupling constants in Hz. Values for the minor isomers are given in parentheses. [b] Coupling constants could not be measured because of overlapping cross peaks in the E. COSY spectrum. [c] The low-field protons are listed first. For the Phe residues the diastereotopic assignments are given.

(32) Wüthrich, K. *NMR of Proteins and Nucleic Acids*; John Wiley: New York, 1986.
(33) Goodman, M.; Mierke, D. F. *J. Am. Chem. Soc.* **1989**, *111*, 3489–3496.

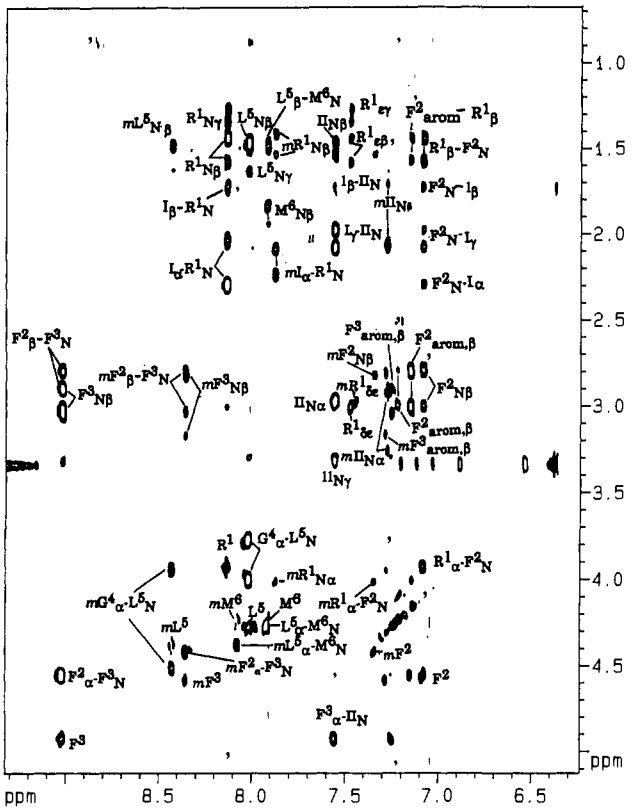

Figure 5. Expanded portion of a NOESY spectrum of SP **2** recorded at 303 K at 600 MHz with a mixing time of 150 ms. The cross peaks from the minor isomer are labeled with an *m*.

Table III. ^2J(H,H) and ^3J(H,H) Proton Coupling Constants of Fragments I and II of Major Isomers of SP **1** and **2** in DMSO at 303 K[a]

	1	**2**
fragment I		
$H^{\alpha 1}$–$H^{\alpha 2}$	−16.3	−13.5
$H^{\alpha 1}$–$H^{\beta 1}$	12.3 (11.8)[b]	5.1 (3.2)[b]
$H^{\alpha 1}$–$H^{\beta 2}$	3.9 (2.6)	8.8 (11.8)
$H^{\alpha 2}$–$H^{\beta 1}$	3.9 (2.6)	7.5 (3.5)
$H^{\alpha 2}$–$H^{\beta 2}$	4.9 (4.1)	5.8 (3.2)
$H^{\beta 1}$–$H^{\beta 2}$	−17.3	*c*
$H^{\gamma 1}$–$H^{\gamma 2}$		−14.5
$H^{\beta 1}$–$H^{\gamma 1}$		6.0 (1.7)[b]
$H^{\beta 2}$–$H^{\gamma 1}$		7.6 (8.3)
$H^{\beta 1}$–$H^{\gamma 2}$		9.3 (8.4)
$H^{\beta 2}$–$H^{\gamma 2}$		5.5 (1.7)
fragment II		
$H^{\gamma 1}$–$H^{\gamma 2}$	−14.5	*c*
$H^{\beta 1}$–$H^{\gamma 1}$	11.5 (11.4)[b]	*c*
$H^{\beta 2}$–$H^{\gamma 1}$	6.2 (5.2)	*c*
$H^{\beta 2}$–$H^{\gamma 2}$	12.0 (11.4)	*c*
$H^{\beta 1}$–$H^{\gamma 2}$	3.6 (1.9)	*c*

[a] Values in Hz, experimental error 0.5 Hz. The low- and high-field protons are indicated with 1 and 2, respectively. These couplings have been independently examined.[51] [b] Calculated $^3J_{H,H}$ coupling constants given in parentheses, see details in text. [c] Coupling constants were not measured because of overlapping resonances.

show that each of the two isomers of SP **1** and **2** contain one intramolecular hydrogen bond: the Phe^3 amide in SP **1** (major) and the Phe^2 amide for the other three molecules.

The $^3J_{NH\text{-}H^{\alpha}C}$ coupling constants were obtained mostly from 1D proton spectra after resolution enhancement recorded at 600 MHz. The coupling constants from amides with overlapping resonances were measured from complementary E. COSY spectra. The measured coupling constants are listed in Table II.

The conformational information of the coupling constants of peptides is usually limited, often suggesting conformational averaging. For this study the $^3J_{NH\text{-}H^{\alpha}C}$ coupling constants were used as conformational constraints only when greater than 8.5 Hz (suggesting a ϕ between −100° and −140°) or less than 5.5 Hz (suggesting a ϕ between 40° and −90°).[34,35] Weak constraints were placed on the ϕ of Phe^2 of all four molecules, on Arg of SP **1** (major) and on Phe^3 of SP **2** (minor).

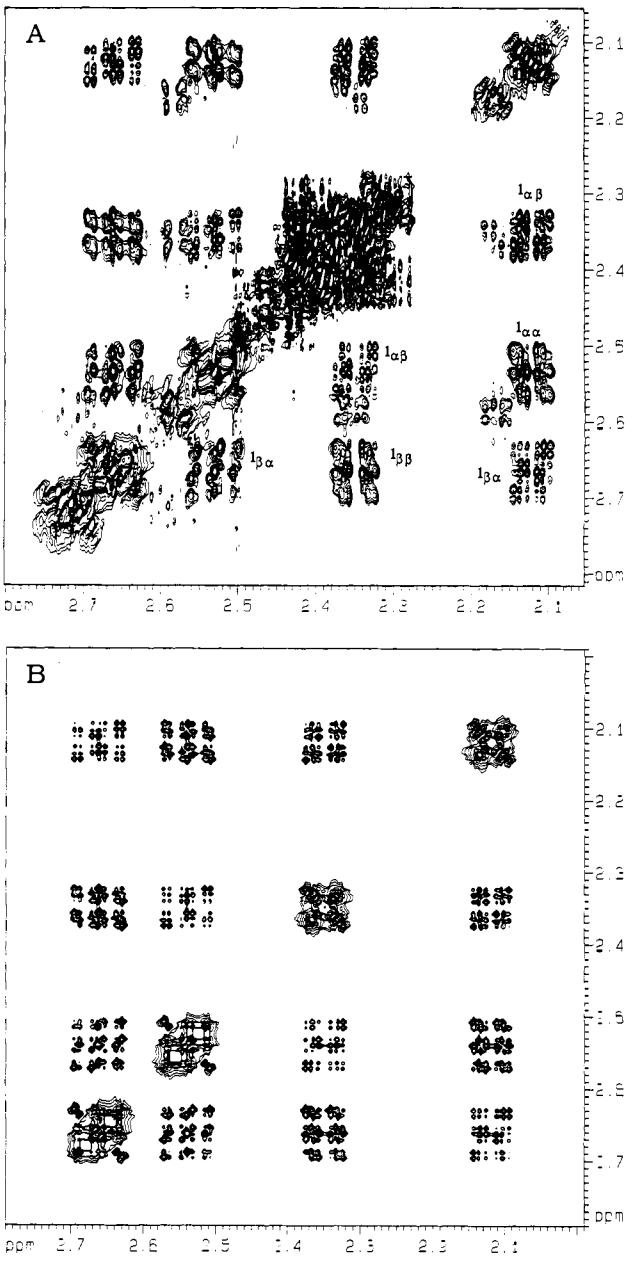

Figure 6. An E. COSY spectrum of SP **1** recorded at 303 K at 500 MHz illustrating the cross peaks of the bridging region (A) and the corresponding simulated spectrum (B).

The $^3J_{C^{\alpha}H\text{-}C^{\beta}H}$ coupling constants were obtained from complementary E. COSY spectra. These coupling constants were extracted for Arg, Phe^2, Phe^3, and Leu and are listed in Table II. A portion of the E. COSY spectrum of SP **1** is shown in Figure 6. In addition, the ^2J and ^3J coupling constants between the $C^{\alpha}H_2$–$C^{\beta}H_2$ and $C^{\beta}H_2$–$C^{\gamma}H_2$ protons of fragments I and II from the bridging region were measured and are given in Table III. It is worthwhile to note the procedure used for the extraction of

(34) Moore, J. M.; Case, D. A.; Chazin, W. J.; Gippert, G. P.; Havel, T. F.; Powls, R.; Wright, P. E. *Science* **1988**, *240*, 314–317.

(35) Different torsional constraints have been suggested. For example, Kline et al. (Kline, A. D.; Braun, W.; Wüthrich, K. *J. Mol. Biol.* **1988**, *204*, 675–694) suggest the following: $^3J_{NH\text{-}H^{\alpha}C} < 5.5$, ϕ between −40 and −90, $^3J_{NH\text{-}H^{\alpha}C} > 8.0$, ϕ between −80 and −160, and $^3J_{NH\text{-}H^{\alpha}C} > 10.0$ ϕ between −100 and −140.

Table IV. Calculated Populations of the Side Chain Rotamers of Phe[2] and Phe[3] of SPI **1** and **2**, Derived from $^3J_{C^\alpha H-C^\beta H}$ Coupling Constants and NOEs[a]

residue	P_I	P_{II}	P_{III}
SP **1**			
Phe[2]	90	2	8
	(8)	(80)	(12)
Phe[3]	54	29	17
	(5)	(72)	(23)
SP **2**			
Phe[2]	57	10	33
	(60)	(15)	(24)
Phe[3]	28	51	21
	(74)	(3)	(23)

[a] The calculated populations for the minor isomers are given in parentheses. The dominant populations P_I ($\chi_1 = -60°$), P_{II} ($\chi_1 = 180°$), and P_{III} ($\chi_1 = 60°$) were evaluated using $^3J_{C^\alpha H-C^\beta H}$ coupling constants and NOEs between NH_i–$C^\beta H_i$, NH_{i+1}–$C^\beta H_i$, and $C^\alpha H_i$–$C^\beta H_i$ protons.

these constants. In general, to obtain the simplest fine structure of E. COSY cross peaks for a given spin system, it is necessary to record and sum up all the possible multiple quantum coherences with appropriate weighting factors.[14,15] However, exploiting the higher proton multiquantum coherences (greater than four) in the E. COSY experiment is complicated by low sensitivity and instrumental difficulties. Nevertheless, it is possible to extract coupling constants for the four spin systems mentioned above by the analysis of the fine structure of cross peaks in the three-spin E. COSY spectrum. First the geminal and vicinal coupling constants of $C^\alpha H,C^\beta H$ and $C^\beta H,C^\gamma H$ protons were obtained from the square structure of direct and displacement vectors of the passive spin–spin coupling of the geminal proton cross peaks. Next, the measured coupling constants were examined by comparing the experimental and simulated E. COSY spectrum for these spin systems. The simulated spectrum for the spin systems of the bridging region of SP **1** is shown in Figure 6B. The good agreement of the fine structures of the cross peaks from the two spectra indicates that the extracted coupling constants are correct. Following a similar approach, the geminal and vicinal coupling constants between $C^\beta H_2$ and $C^\gamma H_2$ protons in fragment II were measured. Unfortunately, it was not possible to obtain these constants for the minor isomers of SP **1** and **2** because of the low concentration and spectral overlap.

The side chains are usually more flexible than the peptide backbone. Nevertheless, it is sometimes possible to identify preferred orientation. From the vicinal coupling constants of amino acids with two β-protons, the populations of these amino acid side chain rotamers can be calculated according to Pachler.[36] The calculated values of the rotamer populations are listed in Table IV. The assignment of the prochiral β-protons was achieved with additional information: the interproton distances from the $C^\alpha H$–$C^\beta H$ and NH–$C^\beta H$ NOEs were used to select one of two possible rotamer sets evaluated from the coupling constants. It was possible to calculate the rotamer populations only for the Phe residues: overlapping β-proton resonances did not permit the selection of one preferred side chain orientation for the remaining residues. A similar procedure was used to evaluate the CO–C^α–C^β–CO (χ_2 fragment I) and C^α–C^β–C^γ–N (χ^3 fragment II) dihedral angles in the bridging region of the major isomer of SP **1**. The vicinal coupling constants (Table III) together with NOEs between NH Arg, NH Phe[2] and the $H^{\alpha 1}$,$H^{\alpha 2}$ protons of fragment I result in values of −60° and −180° for CO–C^α–C^β–CO and C^α–C^β–C^γ–N, respectively. In addition, the quantitative analysis of the NOEs between NH Arg, NH Phe[2] and the bridging region allows for the stereospecific assignment of the H^α and H^β protons of fragment I.

For the quantitative evaluation of the NOEs, the spectra recorded with mixing times of 100 and 150 ms were used for the major and minor isomers, respectively. The longer time for the minor isomer was necessary because of the lower signal-to-noise ratio. The buildup of the NOEs was linear for these mixing times as judged from the NOESYs at different mixing times. The interproton distances were calculated following the assumption that the volume integral of the cross peak is inversely proportional

(36) (a) Pachler, K. G. R. *Spectrochim. Acta* **1963**, *19*, 2085–2092. (b) Pachler, K. G. R. *Spectrochim. Acta* **1964**, *20*, 581–587.

Table V. Distances Calculated from NOESY Spectra of the Major and Minor Isomers of SP **1** and **2** in DMSO at 303 K[a]

atoms		SP **1**		SP **2**	
		major[c]	minor	major[c]	minor
		Interresidue			
Arg[1] H^N	Phe[2] H^N	2.4 (0.7)	2.1	2.5 (−0.4)	2.6
Arg[1] H^N	I $H^{\alpha 1}$	2.2 (0.0)	2.2	2.5 (−0.4)	2.4
Arg[1] H^N	I $H^{\alpha 2}$	2.7 (−0.4)	2.8	3.3 (0.3)	2.5
Arg[1] H^α	Phe[2] H^N	3.1 (−0.5)	3.4	3.1 (0.0)	2.9
Arg[1] $H^{\beta 1}$	Phe[2] H^N	4.0 (0.5)	*b*	3.1 (−0.6)	2.9
Arg[1] $H^{\beta 2}$	Phe[2] H^N	3.5 (0.8)	*b*	3.6 (−0.5)	3.3
Phe[2] H^N	Phe[3] H^N	2.3 (−1.7)	2.7	4.1 (0.1)	2.7
Phe[2] H^N	I $H^{\alpha 1}$	3.3 (−0.7)			
Phe[2] H^N	I $H^{\alpha 2}$	3.4 (−1.6)			
Phe[2] H^N	I $H^{\beta 1}$			3.5 (−1.1)	
Phe[2] H^N	I $H^{\gamma 1}$			3.5 (−0.2)	
Phe[2] H^N	II $H^{\beta 1}$	3.3 (−2.6)			
Phe[2] H^α	Phe[3] H^N	2.9 (0.6)	*b*	2.3 (0.1)	2.3
Phe[2] $H^{\beta 1}$	Phe[3] H^N	3.3 (−1.2)	*b*	*b*	2.7
Phe[2] $H^{\beta 2}$	Phe[3] H^N	3.0 (−1.0)	2.5	3.1 (−0.1)	*b*
Phe[2] $H^{\beta 1}$	II $H^{\beta 1}$	2.9 (−2.0)			
Phe[2] $H^{\beta 2}$	II $H^{\beta 1}$	2.5 (−2.0)			
Phe[2] $H^{\beta 2}$	II $H^{\beta 2}$	3.5 (−2.8)			
Phe[3] H^N	II $H^{\beta 1}$	3.3 (−1.7)			
Phe[3] H^N	II $H^{\gamma 1}$	2.7 (−1.2)			
Phe[3] H^α	II $H^{\beta 1}$			3.2 (−0.8)	
Phe[3] H^α	II $H^{\beta 2}$			2.8 (−1.2)	
Phe[3] H^α	II $H^{\gamma 1}$	2.2 (0.9)		2.2 (−0.9)	
Phe[3] H^α	II $H^{\gamma 2}$	2.6 (−0.3)		2.2 (0.6)	
Gly[4] $H^{\alpha 1}$	Phe[3] H^α		*b*		2.4
Gly[4] $H^{\alpha 2}$	Phe[3] H^α		*b*		2.7
Gly[4] $H^{\alpha 1}$	Leu[5] H^N	2.7 (−0.6)	2.4	2.7 (−0.7)	2.4
Gly[4] $H^{\alpha 2}$	Leu[5] H^N	2.7 (0.6)	2.3	2.6 (0.3)	2.3
Gly[4] $H^{\alpha 1}$	II $H^{\beta 1}$		3.0		
Gly[4] $H^{\alpha 2}$	II $H^{\beta 1}$		3.3		
Gly[4] $H^{\alpha 1}$	II $H^{\beta 2}$		3.2		
Gly[4] $H^{\alpha 2}$	II $H^{\beta 2}$		3.6		
Gly[4] $H^{\alpha 1}$	II $H^{\gamma 1}$	2.8 (−0.6)		*b*	
Gly[4] $H^{\alpha 1}$	II $H^{\gamma 2}$	3.3 (−0.4)		*b*	
Gly[4] $H^{\alpha 2}$	II $H^{\gamma 2}$	2.2 (−0.7)		*b*	2.7
Leu[5] H^α	Met[6] H^N	2.4 (0.1)	2.3	*b*	2.3
Leu[5] $H^{\beta 1}$	Met[6] H^N	3.2 (−0.9)		3.6 (0.8)	
Leu[5] $H^{\beta 2}$	Met[6] H^N	2.5 (−0.5)		3.6 (−0.2)	
I $H^{\beta 1}$	II H^N	2.5 (−2.0)	2.2		
I $H^{\beta 2}$	II H^N	2.2 (−1.9)	2.6	3.9 (−0.3)	
I $H^{\gamma 1}$	II H^N			2.8 (0.2)	
I $H^{\gamma 2}$	II H^N			2.8 (−0.4)	2.3
		Intraresidue			
Arg[1] H^α	H^N	2.8 (0.1)	2.9	2.8 (0.0)	2.9
Arg[1] $H^{\beta 1}$	H^N	3.1 (−0.5)	3.2	3.3 (−0.3)	2.9
Arg[1] $H^{\beta 2}$	H^N	2.5 (0.0)	2.7	2.7 (0.3)	2.6
Phe[2] H^α	H^N	2.9 (0.1)	2.6	3.0 (0.2)	2.7
Phe[2] $H^{\beta 1}$	H^N	3.3 (−0.2)	2.7	3.2 (−0.6)	*b*
Phe[2] $H^{\beta 2}$	H^N	2.4 (0.1)	2.5	2.9 (0.1)	2.9
Phe[3] H^α	H^N	*b*	2.6	2.8 (0.2)	2.8
Phe[3] $H^{\beta 1}$	H^N	2.7 (0.4)	2.4	*b*	2.9
Phe[3] $H^{\beta 2}$	H^N	2.9 (−0.6)	2.6	2.7 (0.3)	*b*
Leu[5] H^α	H^N	2.9 (0.0)	2.7	2.9 (0.0)	2.8
Leu[5] $H^{\beta 1}$	H^N	2.4 (−0.1)	*b*	2.8 (−0.4)	*b*
Leu[5] $H^{\beta 2}$	H^N	3.4 (0.0)	*b*	2.8 (−0.9)	*b*
Met[6] H^α	H^N	2.8 (−0.1)	2.9	2.9 (0.0)	3.0
II H^N	$H^{\alpha 1}$	2.4 (−0.3)	3.0	*b*	2.8
II H^N	$H^{\alpha 2}$	2.5 (−0.3)	2.7	*b*	2.8
II H^N	$H^{\beta 1}$	3.4 (−1.1)		3.4 (−0.1)	3.0
II H^N	$H^{\beta 2}$	3.6 (0.1)		3.2 (0.6)	3.4
II H^N	$H^{\gamma 1}$	3.3 (−0.1)			

[a] Distances in Å. The nomenclature of the fragments of the bridging region is shown in Figure 1. [b] Distances could not be determined because of overlapping signals. [c] The values in parentheses are the difference between the distances from the NOE data and the calculated effective distance during the continuation of the simulation without experimental constraints ($dis_{NOE} - dis_{free}$).

to the sixth power of the distance. The cross peak between the geminal NGly protons with an assumed interproton distance of 1.78 Å was used as a reference. The mean value of the two distances obtained from the NOE cross peaks, which are symmetric about the main diagonal, was used and these values are listed in Table V.

In general the cis/trans isomer exchange rate is slow on the NMR time scale (barrier of the order of 70–80 kJ/mol).[37] On the other hand, the time of transition between cis and trans isomers is extremely short and we can approximate this process as a fast switching between two discrete states with different populations;[37a] thus, from a thermodynamic point of view, it is possible to avoid the characterization of the transition between the cis and trans isomers. Such a model has often been used to describe cis and trans isomers separately. In this study, the NMR parameters (coupling constants and line width of proton resonances) were unchanged at elevated temperatures, indicating that this approach is appropriate. Therefore, restrained MD simulations were performed for the cis and trans isomers independently.

The averages of the torsions during the MD simulations with NOE and dihedral restraints are given in Table VI. The average structures during the 100 ps were calculated and energy minimized for 200 steps of steepest descents. The resulting conformations are shown in Figure 7. For the major isomers of SP **1** and **2** the experimental restraints were turned off and the simulation continued for 400 ps. The average torsion values were calculated and the differences between this "free" simulation and that with application of the experimental constraints are included in Table VI. The standard deviations of the torsions during the restrained and free MD simulations for the major isomers are given in the supplementary material (Table S5).

From the free MD simulations the NOEs were monitored by calculating the effective distance, $\langle r^{-3}\rangle^{-1/3}$, averaged over the trajectory. The difference of the effective distance calculated from the free simulation and the target distance derived from the NOEs is included in Table V.

Discussion

NOE-Restrained Molecular Dynamics. The average structure from the 100 ps of restrained MD of the major isomer of SP **1**, partially energy minimized, is shown in Figure 7A. The conformation is well-determined from the experimental data. The backbone coupling constants of Arg and Phe^2 limit the ϕ dihedral of these residues. The NOEs suggest the cyclic portion of the molecule is compact; especially important are the cross ring NOEs, namely, Phe^2 NH to the bridging region I $C^{\alpha}H_2$ and II $C^{\beta}H_2$ and Phe^2 $C^{\beta}H$ and Phe^3 NH to fragment II of the bridging region. The N_iH–$N_{i+1}H$ NOEs for Arg and Phe^2 force the amide protons close together, directed toward the ring system. A hydrogen bond between the Phe^3 NH and Arg O, which is consistent with a γ-turn about Phe^2, exists for 61% of the simulation. A hydrogen bond between the Phe^2 NH and the $^{\alpha}$CO of fragment I, forming a γ-turn about the Arg, exists for 26% of the simulation. However, both of these turn structures are disfavored by the small distance between the amides of Arg and Phe^2 as well as Phe^2 and Phe^3 with calculated distances of 2.4 and 2.3 Å, respectively. The above-mentioned hydrogen bond, or at least a shielding from solvent, is in accord with the small temperature coefficients (Table I). The average restraint violation of the NOEs during the simulation is 0.20 Å. This is a rather large value for cyclic peptides. The largest violation is from the Arg NH–Phe^2 NH NOE (average distance 3.0 Å) because of the different hydrogen-bonding patterns. The conformation of the linear portion of the molecule, NGly-Leu-Met-NH_2, remains extended during the simulations. The side chain conformation of Phe^2 (average value of −64°) is in agreement with the large population calculated from the coupling constants (90% for $\chi_1 = -60°$). For the Phe^3 side chain an average value of −68° is found during the simulations; the calculated populations indicate a small preference for the −60° rotamer (Table IV).

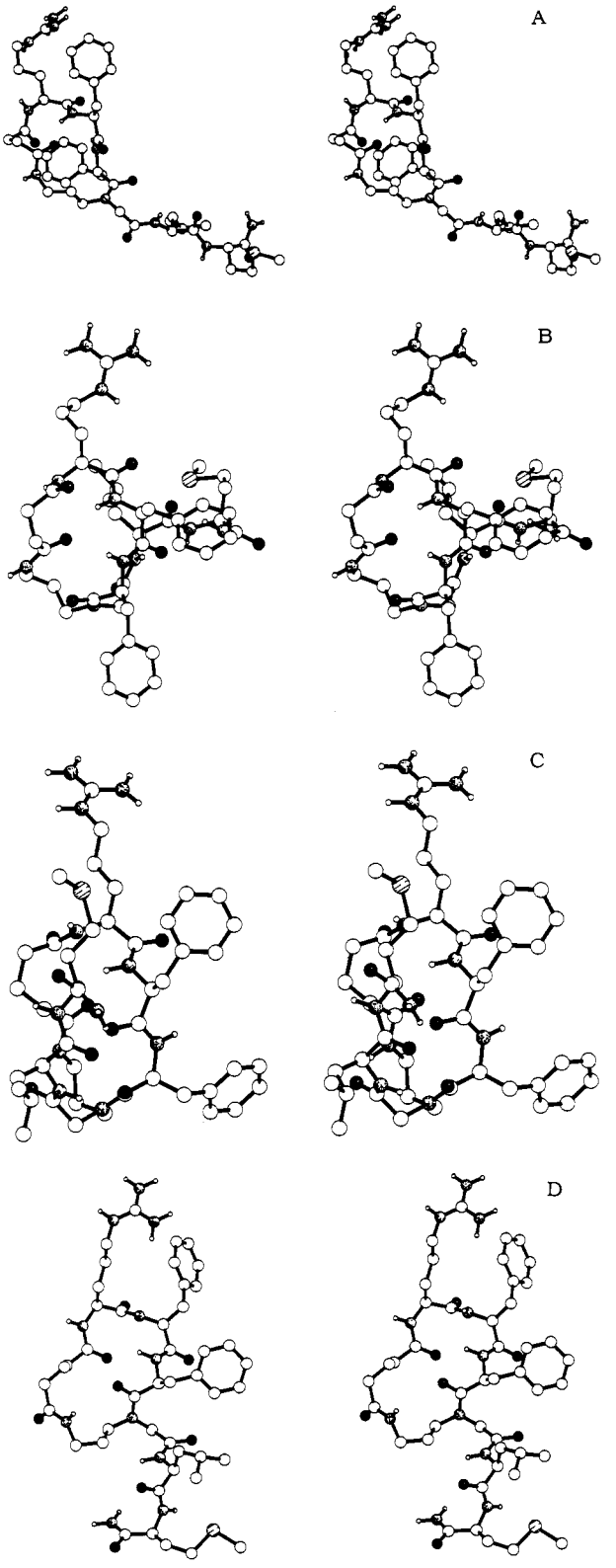

Figure 7. Stereoplot of the partially minimized average structure from the restrained molecular dynamics simulations of SP **1** and **2**: (A) the major (trans) isomer of SP **1**, (B) the minor (cis) isomer of SP **1**, (C) the major (trans) isomer of SP **2**, and (D) the minor (cis) isomer of SP **2**.

The average structure from the restrained MD simulation of the minor isomer of SP **1**, partially energy minimized, is shown in Figure 7B. The cis isomer, in contrast to the trans (major) isomer, is not compact but extended: there are no NOEs across

(37) (a) Kessler, H. *Angew. Chem., Int. Ed. Engl.* **1970**, *9*, 219–235. (b) Stewart, W. E.; Siddall, T. H. *Chem. Rev.* **1970**, *70*, 517–551. (c) Grathwohl, C.; Wüthrich, K. *Biopolymers* **1981**, *20*, 2623–2633. (d) Mierke, D. F.; Yamazaki, T.; Said-Nejad, O. E.; Felder, E. R.; Goodman, M. *J. Am. Chem. Soc.* **1989**, *111*, 6847–6849.

Table VI. Averages of Dihedral Angles from Molecular Dynamic Simulations of the Trans and Cis Isomers of SP **1** and **2** in DMSO

torsion		SP 1		SP 2	
		trans[a]	cis	trans[a]	cis
Arg	ϕ	−71.3 (−21.3)	64.0	−103.1 (−2.5)	−13.6
	ψ	−14.6 (26.6)	−14.7	−13.0 (−12.4)	−78.4
	χ_1	−64.1 (1.9)	−84.2	−70.3 (0.7)	−161.8
Phe^2	ϕ	−112.7 (−37.5)	−123.3	−131.3 (9.2)	−115.9
	ψ	60.4 (−29.0)	−55.1	124.3 (−4.3)	1.6
	χ_1	−64.3 (11.7)	−173.8	−69.1 (2.5)	−78.2
Phe^3	ϕ	−35.1 (39.4)	−120.5	−1.4 (34.7)	−151.2
	ψ	112.8 (−12.4)	103.6	119.4 (−9.2)	121.8
	χ_1	−67.8 (5.1)	−174.9	−74.7 (0.7)	−75.1
NGly	ϕ	−60.9 (1.0)	−117.8	73.4 (−3.2)	78.6
	ψ	127.3 (18.8)	86.8	−94.5 (7.5)	55.7
Leu	ϕ	−168.1 (−43.0)	−141.1	−131.4 (−13.3)	−164.0
	ψ	142.4 (−12.8)	98.6	149.2 (4.4)	86.1
	χ_1	−152.0 (4.9)	−172.4	62.1 (6.7)	−155.7
Met	ϕ	−107.8 (4.9)	71.5	−78.8 (18.2)	53.3
	ψ	95.5 (−2.6)	−48.9	82.2 (−33.0)	42.8
	χ_1	−170.2 (−7.8)	−79.0	−167.3. (2.7)	−75.2
I	χ_1	−76.4 (57.6)	−88.3	−118.2 (11.6)	−68.7
	χ_2	−54.5 (14.1)	−72.4	61.1 (−12.6)	−178.7
	χ_3	−100.3 (137.9)	−115.6	−95.7 (−6.9)	61.4
	χ_4			95.7 (40.9)	77.1
II	χ_1	60.2 (−113.0)	51.3	144.0 (−52.8)	116.6
	χ_2	−153.6 (−84.3)	58.3	−81.4 (0.9)	−74.1
	χ_3	166.9 (10.6)	−112.7	79.4 (68.9)	160.3
	χ_4	89.0 (19.8)	−86.3	57.2 (−43.3)	101.2

[a] The values in parentheses are the difference between the averages found for the restrained and free MD simulations ($Tor_{restrained} - Tor_{free}$). The definitions of the torsions of the bridging region are as follows—Fragment I: χ_1 NH–CO–C^α–C^β, χ_2 CO–C^α–C^β–CO, χ_3 C^α–C^β–CO–NH (SP **1**) or C^α–C^β–C^γ–CO (SP **2**), χ_4 C^β–C^γ–CO–NH (SP **2** only). Fragment II: χ_1 CO–NH–C^α–C^β, χ_2 NH–C^α–C^β–C^γ, χ_3 C^α–C^β–C^γ–N(NGly), χ_4 C^β–C^γ–N(NGly)–C^α(NGly).

the ring system. However, the N_iH–$N_{i+1}H$ NOEs for Arg and Phe^2 are very similar for the two isomers. The amide proton of Phe^2 is directed toward the ring system during the simulation forming hydrogen bonds with the $^\alpha$CO and $^\beta$CO of the I fragment for 66 and 26% of the simulation, respectively. The amide of Phe^3 has the proper distance to form a hydrogen bond with the $^\beta$CO of fragment I but the angle is too small: this hydrogen bond is found only in 8% of the simulation. The average distance restraint violation is 0.11 Å, indicating an equilibrium between structures with different hydrogen-bonding patterns. The side chain rotamers of the two Phe's are trans, in agreement with the large populations of this rotamer calculated from the coupling constants.

The major isomer of SP **2**, similar to the major isomer of SP **1**, has many NOEs across the cyclic portion of the peptide, namely, Phe^2 NH to the bridging region I $C^\beta H_2$ and I $C^\gamma H_2$ and Phe^3 $C^\alpha H$ to the II fragment of the bridging region. The average structure from 100 ps of restrained MD, partially minimized, is shown in Figure 7C. The N_iH–$N_{i+1}H$ NOEs for Arg and Phe^2 as observed for the major isomer of SP **1** are also found with SP **2**. However, the Phe^2 NH–Phe^3 NH NOE is much weaker, suggesting a much greater distance (4.1 Å compared to 2.3 Å for SP **1**). This keeps the Arg and Phe^2 amide protons oriented toward the ring system while the Phe^3 amide is directed toward the solvent. The hydrogen bond between Phe^2 NH and $^\alpha$CO, forming a γ-turn about the Arg, is not found during the simulation. As with the major isomer of SP **1**, this structure is disfavored by the small distance between the amides of Arg and Phe^2. A hydrogen bond between the Phe^2 NH and $^\gamma$CO of fragment I exists for 26% of the simulation. The average restraint violation of the NOEs during the simulation is 0.08 Å. As with both isomers of SP **1**, the linear portion of the peptide remains extended during the simulations. Both of the Phe side chains populate the −60° rotamer during the simulation while the side chain coupling constants indicate conformational averaging with a slight preference for the −60° and 180° rotamers for Phe^2 and Phe^3, respectively.

The average structure from the restrained MD of the minor isomer of SP **2**, partially energy minimized, is shown in Figure 7D. It is the least well experimentally determined structure, not surprising since it accounts for only 18% of the population. There are no NOEs across the cyclic portion of the molecule; in fact, all of the NOEs besides the N_iH–$N_{i+1}H$ of Arg and Phe^2 are intraresidue or sequential. The Phe^2 amide is involved in a hydrogen bond with the $^\alpha$CO of fragment I, corresponding to a γ-turn about Arg, for 48% of the simulation. The amide of Phe^3 is also involved in a hydrogen bond, with $^\gamma$CO of fragment I, in a small percentage of the simulation (19%). The large NOE violation of 0.18 Å can be attributed to the Arg NH–Phe^2 NH NOE and the equilibrium between the γ-turn and fulfillment of this NOE. The side chain rotamers for the Phe residues are −60° in agreement with the populations predicted from the coupling constants.

The MD simulations described here were carried out with DMSO as the solvent. The potential energy parameters for DMSO have recently been developed for use within the GROMOS force field.[8,25] The importance of solvent within simulations to avoid the so called "in vacuo" effects has been well-documented.[38] The DMSO does not form a solvent sphere or shell around the peptide during the simulation, as is often found with water as the solvent.[38b] Only a few DMSO molecules, those in close proximity to charged groups of the peptide, have preferred orientations. The remainder of the DMSO molecules adopt configurations very much like that of the pure solvent.[39] Snapshots of the structures after 400 ps of free MD simulation including the DMSO molecules that participate in intermolecular hydrogen bonds are shown in Figure S3 (supplementary material). The formation of intermolecular hydrogen bonds between DMSO and amide protons has been shown to be a strong stabilizing force during the simulations of model peptide compounds.[8]

Quality of Structures. It is important to judge the quality of structures obtained by restrained MD simulations. Usually, as was used here, the number and size of the distance-constraint violations have been exploited as a measure for the agreement between the model structure and NMR data. Recently an NMR R factor[40] was introduced which measures the deviation between experimental NOEs and those calculated for the final structure. However, such an approach has, as the authors note, a disadvantage because local mobility within the molecule is neglected in the theoretical calculations. On the other hand, it is known that the accurate interpretation of NOEs,[41-43] *J*-coupling constants,[43-46] or relaxation parameters[47] for nonrigid molecules is possible only by using a dynamic model. However, with the computing power and experimental techniques currently available this is not possible to do rigorously.

We propose a method for examining the stability of the obtained structures by extended, free MD simulations in solvent: a continuation of the MD calculation (starting with the structure from the restrained simulation) with no experimental constraints. The differences between the experimental (NOE-derived interproton distances and *J*-coupling constants) and theoretical NMR parameters produced from the trajectory of the peptide in the free MD simulation is a measure of the quality of obtained structure (assuming that the energetic force field is an accurate description of the peptide and solvent). Therefore, free MD simulations of 400 ps of the major isomers of SP **1** and **2** in DMSO were performed. It is important to note that this procedure is not possible

(38) (a) van Gunsteren, W. F.; Berendensen, H. J. C. *Angew. Chem., Int. Ed. Engl.* **1990**, *29*, 992–1023. (b) Smith, P. E.; Dang, L. X.; Pettitt, B. M. *J. Am. Chem. Soc.* **1991**, *113*, 67–73. (c) Kurz, M.; Mierke, D. F.; Kessler, H. *Angew. Chem., Int. Ed. Engl.* **1992**, *31*, 210–212.
(39) Itoh, S.; Ohtaki, H. *Z. Naturforsch.* **1987**, *42a*, 858–862.
(40) Gonzalez, C.; Rullmann, J. K. C.; Bonvin, M. J. J.; Boelens, R.; Kaptein, R. *J. Magn. Reson.* **1991**, *91*, 659–664.
(41) Trapp, J. *J. Chem. Phys.* **1980**, *72*, 6055–6063.
(42) Saulitis, J.; Liepins, E. *J. Magn. Reson.* **1990**, *87*, 80–91.
(43) Kessler, H.; Griesinger, C.; Müller, A.; Lautz, J.; van Gunsteren, W. F.; Berendsen, H. J. G. *J. Am. Chem. Soc.* **1988**, *110*, 3393–3396.
(44) Byrstrov, V. F. *Prog. Nucl. Magn. Reson. Spectrosc.* **1976**, *10*, 41–81.
(45) Kessler, H. *Angew. Chem., Int. Ed. Engl.* **1982**, *21*, 512–523.
(46) Jardetzky, O. *Biochem. Biophys. Acta* **1980**, *621*, 227–235.
(47) (a) Lipari, G.; Szabo, A. *J. Am. Chem. Soc.* **1982**, *104*, 4546–4559. (b) Lipari, G.; Szabo, A. *J. Am. Chem. Soc.* **1982**, *104*, 4559–4570.

with in vacuo calculations because restraints from experimental data are usually necessary to mimic the influence of the solvent.[48] Of course, free simulations have been performed previously, but have not been used as a quantitative test of the quality of derived structures.

The relatively small deviations of the dihedral torsion angles in the free MD simulation (Table VI) indicate that both structures are energetically stable. The standard deviations from the restrained and free simulations indicate greater mobility of fragments I and II and the Leu and Met amino acids. The bridging region of SP **1** and **2** is more conformationally flexible than the rest of the cyclic portion of the molecule because of the aliphatic CH_2–CH_2 fragments while the larger mobility of the Leu and Met amino acids can be associated with their location outside of the cycle. Of course, local changes in conformation must have an effect on NMR parameters, and in order to examine these effects the vicinal J coupling constants between the H^{α},H^{β} and H^{β},H^{γ} protons of the bridging region (Table III) and the NOE-derived distances (Table V) were calculated from the free MD simulation. The calculated vicinal J-coupling constants reproduce the experimental values for SP **1** better than for SP **2**, which correlates with the larger changes of the χ_2 and χ_3 dihedral angles in fragment I of SP **2**. It is surprising that the dihedral angles χ_2 of fragment I and χ_3 of fragment II of SP **1** remain almost unchanged during the free MD simulation (Table VI).

A more stringent test is a comparison of the distances derived from the experimental NOEs and effective interproton distances, $\langle r^{-3}\rangle^{-1/3}$, produced from the free MD simulation. In the case of fast intramolecular flexibility, when the intramolecular motion is faster than the time of the overall reorientation of the molecule, the observed NOE according to Tropp[41] is proportional to the average value $\langle r^{-3}\rangle^{2}$: this was used in calculating the interproton distances from the experimental NOEs. This assumption holds true when the correlation functions for the motion of the different interproton vectors are similar. The calculated interproton distances, given in Table V, reproduce the experimental ones quite well for the conformationally stable Arg-Phe[2]-Phe[3]-NGly part of the molecule while relatively large differences between these distances are observed for the protons of the bridging region. The reason for this could be different mobilities of proton pairs in this part of the molecule, and as a result, the assumption about equal correlation times is not valid. The different mobilities would also introduce error into the experimentally derived distances since they were calculated assuming a rigid structure using a two-spin approximation. Preliminary results using the iterative full relaxation matrix approach (IRMA)[49] indicate only minor changes in the list of distance restraints, suggesting that spin diffusion is not responsible for the observed discrepancy. Other possible explanations are the limited time of the free simulation (400 ps) or a deficiency in the energetic force field to properly reproduce the aliphatic portion of these conformationally constrained ring systems. The constrain is particularly evident in fragment I of SP **1** with only two methylenes between peptide bonds: this constraint may lead to molecular motions and dynamics different than that for the remainder of the molecule.

Biological Relevance. The cyclization of the SP analogues was successful: the activity profiles of SP **1** and **2** are similar to that of the WS Septide. It is important to realize the significance of this result: a large number of conformations excessible to the linear analogue have been excluded by the cyclization, and yet the analogues maintain the biological activity. As our NMR studies indicate, the Phe-N(γ-aminobutylene)Gly peptide bond adopts both a cis and a trans orientation. From the NMR and computer simulations, the conformation of both of the isomers has been determined. However, these studies did not indicate which of the two ring conformations relates to the bioactive conformation that selectively activates the NK-1 receptor.

The conformation of SP **2** illustrates similarities with the conformation found for the linear WS Septide.[7] However, it must be stressed that the cyclization was designed from molecular modeling to maintain the conformation observed for the WS Septide. The conformation of the WS Septide was dominated by a β-I turn about the Pro-Leu residues. Of course, in the cyclic analogues this turn is not possible. However, the orientation of the phenylalanines in the two molecules is quite similar. These residues, numbers 7 and 8 in native SP, are important in the selectivity of peptide analogues for the different NK receptors. For activity at the NK-1 receptor both phenylalanines are necessary while the second phenylalanine is replaced with a valine to enhance the NK-2 activity and is N-methylated to enhance the activity at the NK-3 receptor.[3e,7]

The SP **2** analogue is 15 times more active than SP **1** at the NK-1 receptor, indicating that some flexibility is required for biological activity. Other cyclic peptides of this series which are more constrained (i.e. containing an additional peptide bond in the bridging region) are much less biologically active or even inactive. This finding could indicate two things: (1) to elicit a biological response the substrate must contain some inherent flexibility (e.g. for docking) or (2) the optimal conformation for activity is locked out by the additional constraint. It is important to stress that only the Arg-Phe-Phe region of the peptide is constrained within this series of peptides; the Leu-Met-NH_2, also necessary for biological activity, is conformationally free. Of course, the next step is to constrain this portion of the molecule and work along these lines is in progress: we have used the conformations derived here to design bicyclic analogues in which both halves of the SP hexapeptide are constrained.

Conclusions

The conformation of two NK-1 receptor selective cyclic substance P analogues has been examined in DMSO by NMR and MD simulations. Both analogues exist in an equilibrium of trans and cis isomers about the substituted amide of glycine. The trans isomers have larger populations (78 and 82% for SP **1** and **2**, respectively) and therefore are conformationally better determined because of the larger number of experimental constraints derived from the NMR data. The conformational differences between the major isomers of SP **1** and **2**, differing by the addition of one methylene, illustrate the constrain within the 18- and 19-membered-ring systems. Indeed, there are significant conformational differences of the ring systems between the cis and trans isomers of the analogues.

In order to evaluate the quality of the structures from NMR and restrained MD, the simulation of the major isomers of SP **1** and **2** was continued without the experimental constraints (free) in order to reproduce the dynamical state of these molecules in DMSO. The NOE-derived distances and vicinal spin–spin coupling of the bridging region were calculated from the trajectory of the free MD. The rather good reproducibility of these NMR parameters by such "back-calculation" indicates the energetic stability and quality of obtained structures. The application of this method could be regarded as a tool to test the quality of structures obtained by restrained MD calculations. However, the data presented here show that more stringent and precise procedures for calculating the NOEs should be used (e.g. calculation of correlation functions for each interproton vector motion)[50] to simulate more exactly the dynamics of the mobile parts of the molecule. Such an approach may produce stimuli to improve MD simulation techniques for systems in a solvent and offer opportunities to test the NMR-derived structures of molecules in solution.

Acknowledgment. We gratefully acknowledge the Alexander von Humboldt Stiftung for a fellowship to J.S., the Fulbright Commission for a research award to D.F.M., and financial support

(48) Kessler, H.; Wein, T. *Liebigs Ann. Chem.* **1991**, 179–184.

(49) (a) Boelens, R.; Koning, T. M. G.; Kaptein, R. *J. Mol. Struct.* **1988**, *173*, 299–308. (b) Boelens, R.; Koning, T. M. G.; van der Marel, G. A.; van Boom, J. H.; Kaptein, R. *J. Magn. Reson.* **1989**, *82*, 290–308.

(50) van Gunsteren, W. F.; Karplus, M. *Biochemistry* **1982**, *10*, 2259–2274.

(51) Mronga, S.; Hahn, R. *J. Magn. Reson.* **1991**, *95*, 373–381.

from the Deutsche Forschungsgemeinschaft and Fonds der Chemischen Industrie.

Supplementary Material Available: Tables of proton and carbon shifts of SP **1** and SP **2** and standard deviations of dihedral torsions from molecular dynamic simulations of the trans isomers of SP **1** and **2** and figures giving a NOESY spectrum of SP **1**, an inverse ^1H-^{13}C HMQC spectrum of SP **1**, and stereoplots of SP **1** and SP **2** (9 pages). Ordering information is given on any current masthead page.

Observation of Hydroxyl Protons of Sucrose in Aqueous Solution: No Evidence for Persistent Intramolecular Hydrogen Bonds

Bruce Adams and Laura Lerner*

Contribution from the Department of Chemistry, University of Wisconsin, Madison, Wisconsin 53706. *Received August 26, 1991*

Abstract: We have measured temperature coefficients of the chemical shifts, scalar coupling constants, and exchange rates for the hydroxyl protons in sucrose in mixtures of water and acetone. The values measured are virtually the same for all the hydroxyl protons in sucrose. These observations indicate that there are no persistent hydrogen bonds in sucrose in aqueous solution.

Introduction

The solution conformation of sucrose (Figure 1) remains the subject of continuing interest. An early interpretation of proton NMR data and hard sphere exoanomeric calculations was that the solution structure was "rather rigid", being essentially the same as the crystal structure, including the persistence in solution of the OH-1^f to O-2^g hydrogen bond seen in the crystalline solid.[1] Detailed ^{13}C relaxation and NOE studies have been interpreted similarly as supporting a rigid conformation in solution.[2,3]

More recently, several groups have begun to question the rigidity of sucrose in aqueous solution. Perez and co-workers[4] have argued that the observed proton-proton NOEs are not consistent with any single conformation. Using molecular mechanics and molecular dynamics, Petillo[5] and Tran and Brady[6] have found several conformations for sucrose lower in energy, by ~10 kJ/mol, than the crystal structure. Most recently, Poppe and van Halbeek have demonstrated further discrepancies between proton NOEs and ROEs actually observed and those predicted for a rigid molecule.[7]

If sucrose were to have a rigid structure in aqueous solution, and particularly one other than the most stable conformation, some means of maintaining this structure must be found. The most likely candidate would be one or more interresidue hydrogen bonds, as is seen in the crystal structure and in nonaqueous solution.[1,8] However, Williams and co-workers have recently calculated the energetics of a hydroxyl-to-hydroxyl hydrogen bond to be virtually the same as that for a hydroxyl-to-water bond.[9] This makes it questionable whether the interresidue hydrogen bonds could in fact supply the needed stabilization.

High-resolution NMR has been used in several different ways to infer the existence of hydrogen bonds. (i) In studies of model compounds such as alcohols, it has been observed that hydrogen bonding causes a downfield change in chemical shifts of the involved protons, and that increasing temperature causes an upfield change.[10] Some previous studies have reported smaller temperature coefficients for hydrogen-bonded hydroxyl protons in sugars.[11,12] (ii) Coupling constants and nuclear Overhauser enhancement (NOE) measurements may be used to establish whether or not a particular hydrogen bond is sterically possible. (iii) Further indirect evidence may come from the correlation times of ^{13}C nuclei, if intramolecular hydrogen bonds restrict their motions.[1-3]

Until recently these types of information were obtainable only from ring protons or carbons, or from hydroxyl protons in nonaqueous solution, because of the difficulty in observing hydroxyl protons. But inferring the existence of hydrogen bonds from indirect evidence is not infallible. For example, while relaxation times can be used to detect restricted motion, the restriction may arise from something other than an intramolecular hydrogen bond. Ideally, the most direct evidence for hydrogen bonds would come from NMR parameters for nuclei directly involved in the hydrogen bond.

It has been difficult to observe directly the hydroxyl protons in H_2O because of their rapid exchange with bulk water, as well as the dynamic range problem of observation in H_2O. Recently, several groups have reported success in observing these elusive protons, by lowering the temperature to slow exchange, and by using pulse sequences that suppress the water signal.[12-14] We have used ^1H NMR of hydroxyl protons to seek evidence for intramolecular hydrogen bonds in sucrose in mixtures of water and acetone-d_6.

* To whom correspondence should be addressed.

(1) Bock, K.; Lemieux, R. U. *Carbohydr. Res.* **1982**, *100*, 63.
(2) McCain, D. C.; Markley J. L. *J. Am. Chem. Soc.* **1986**, *108*, 4259.
(3) McCain, D. C.; Markley, J. L. *J. Magn. Reson.* **1987**, *73*, 244.
(4) du Penhoat, C. H.; Imberty, A.; Roques, N.; Michon, V.; Mentech, J.; Descotes, G.; Pérez, S. *J. Am. Chem. Soc.* **1991**, *113*, 3720.
(5) Petillo, P. Personal communication. The calculation was performed using the MM2 program (Allinger, N. L.; Yuh, Y. H. *Quantum Chem. Program Exch. Bull.* **1984**, *4*, 113).
(6) Tran, V. H.; Brady, J. W. *Biopolymers* **1990**, *29*, 961.
(7) Poppe, L.; van Halbeek, H. *J. Am. Chem. Soc.*, in press.
(8) Christofides, J. C.; Davies, D. B. *J. Chem. Soc., Chem. Commun.* **1985**, 1533.
(9) Cox, J. P. L.; Nicholls, I. A.; Williams, D. H. *J. Chem. Soc., Chem. Commun.* **1991**, 1295.
(10) Pople, J. A.; Schneider, W. G.; Bernstein, H. J. *High Resolution Nuclear Magnetic Resonance*; McGraw-Hill Book Company, Inc.: New York, 1959.
(11) St.-Jacques, M.; Sundarajan, P. R.; Taylor, K. J.; Marchessault, R. H. *J. Am. Chem. Soc.* **1976**, *98*, 4386.
(12) Poppe, L; van Halbeek, H. *J. Am. Chem. Soc.* **1991**, *113*, 363.
(13) Leeflang, B. R.; Vliegenthart, J. F. G. *J. Magn. Reson.* **1990**, *89*, 615.
(14) Adams, B.; Lerner, L. In *Oligosaccharide and Polysaccharide Structural Determination by Modern Mass Spectrometry and NMR Spectroscopy*; Cumming, D., Reinhold, V., Eds.; ACS Symposium Series; American Chemical Society: Washington, DC, in press.

0002-7863/92/1514-4827$03.00/0